30-mW-Class High-Power and High-Efficiency Blue Semipolar ($10\bar{1}\bar{1}$) InGaN/GaN Light-Emitting Diodes Obtained by Backside Roughening Technique

Yuji Zhao[1]*, Junichi Sonoda[2], Chih-Chien Pan[2], Stuart Brinkley[1], Ingrid Koslow[2], Kenji Fujito[3], Hiroaki Ohta[2], Steven P. DenBaars[1,2], and Shuji Nakamura[1,2]

[1]*Electrical and Computer Engineering Department, University of California, Santa Barbara, CA 93106, U.S.A.*
[2]*Materials Department, University of California, Santa Barbara, CA 93106, U.S.A.*
[3]*Optoelectronic Laboratory, Mitsubishi Chemical Corporation, Ushiku, Ibaraki 300-1295, Japan*

Received August 19, 2010; accepted August 26, 2010; published online September 17, 2010

The first 30-mW-class semipolar blue light-emitting diode (LED) on a free-standing ($10\bar{1}\bar{1}$) GaN substrate has been demonstrated by using microscale periodic backside structures. The light extraction efficiency and corresponding output power were greatly enhanced, by up to 2.8-fold (bare chip) compare with conventional devices. At a driving current of 20 mA, the LED showed an output power of 31.1 mW and an external quantum efficiency of 54.7%. Semipolar GaN LED technology is now comparable to commercial *c*-plane blue LED technology, not only in terms of internal material properties but also in terms of chip processing techniques.

DOI: 10.1143/APEX.3.102101

Wurtzite (Al,Ga,In)N-based light-emitting diodes (LEDs) have attracted considerable attention since their first demonstration in the early to mid-1990s[1] for their wide applications including traffic signals, full-color displays, backlighting sources for liquid-crystal displays, and general lighting. Although device performance has improved steadily, current commercially available *c*-plane optoelectronic devices suffer from internal electric fields due to discontinuities in both spontaneous and piezoelectric polarization at the heterointerface. This leads to the separation of electrons and holes in the quantum wells and thus limits the radiative recombination rate.[2–5] On the other hand, devices grown on nonpolar planes such as the ($1\bar{1}00$) *m*-plane and ($11\bar{2}0$) *a*-plane, as well as devices grown on ($11\bar{2}\bar{2}$) and ($10\bar{1}\bar{1}$) semipolar planes have been demonstrated with eliminated or reduced polarization fields.[6–13] and are theoretically predicted to have a higher optical gain than *c*-plane devices, due to their anisotropic band structure.[14] Despite those advantages, however, the output power and efficiency of current semipolar and nonpolar LEDs are still lower than those of the best reported *c*-plane devices, mainly due to the poor light extraction efficiency (η_{extr}) compared with their polar counterparts.[15–19]

Light extraction efficiency has become the most important limiting factor for the efficiency of LEDs, since the internal quantum efficiency (IQE) of nitride-based LEDs has been greatly improved (more than 80%)[20] by the availability of low-dislocation GaN substrates and advances in metal organic chemical vapor deposition (MOCVD) techniques. The low η_{extr} is primarily caused by the low critical angle (23°) of the light escape cone, due to the large differences between the refractive indices of GaN ($n \sim 2.5$) and air ($n = 1$).[21] For *c*-plane devices, both η_{extr} and the corresponding output power have been greatly improved by surface roughening methods such as patterned sapphire substrate (PSS) and photoelectrochemical (PEC) etching techniques.[21–25] Semipolar and nonpolar devices, however, still suffer from low light extraction efficiency due to the lack of proper roughening techniques, which have hindered their performance. Recently, Zhong *et al.* have demonstrated that surface patterning with conical features by inductively coupled plasma (ICP) etching could be potentially applied to achieve relatively high power and high efficiency semipolar devices.[26] In this work, we report for the first time a blue semipolar ($10\bar{1}\bar{1}$) InGaN/GaN LED with extremely high output power and efficiency, using an optimized backside roughening technique. The density and size of the conical features were determined to enhance the light extraction efficiency. A light extraction simulation with Monte Carlo ray tracing is also presented.

LED epitaxial layers were homoepitaxially grown by conventional MOCVD on free-standing ($10\bar{1}\bar{1}$) GaN substrates, supplied by Mitsubishi Chemical. The device structure consists of a 1 μm Si-doped n-type GaN layer, three periods of InGaN/GaN multiple quantum wells (MQWs), a Mg-doped 16 nm $Al_{0.15}Ga_{0.85}N$ electron blocking layer (EBL), and a 60 nm p-type GaN layer.[18] For the ($10\bar{1}\bar{1}$) LED fabrication, a rectangular mesa pattern (490×292 or $2000 \times 500\,\mu m^2$) was formed by conventional lithography and chlorine-based ICP etching after an indium tin oxide (ITO) current spreading layer was deposited by electron beam evaporation. Ti/Al/Ni/Au n-type contacts and Ti/Au pads were deposited by electron beam evaporation and a conventional lift-off process. After that, the backsides of the devices were polished and patterned with conical features by conventional contact lithography, followed by ICP etching. The RF source bias power and the BCl_3 to Cl_2 ratio during the ICP etching were intentionally controlled to result in a 58° sidewall inclination angle.[26] The schematic structure of the device with the roughened backside is shown in Fig. 1(a), while scanning electron microscopy (SEM) images of the backside of the GaN substrate before [Fig. 1(b)] and after [Fig. 1(c)] backside roughening are also presented.

Two different experimental series were carried out to maximize η_{extr}. Firstly, circular features with the same top diameter ($\phi = 3\,\mu m$) but different feature densities ($\rho = 5.8 \times 10^5$, 9.0×10^5, and $1.6 \times 10^6\,cm^{-2}$) were patterned, and on-wafer light output power results were measured from the backside of these devices using a broad-area silicon photodiode. In the second experiment, the same measurements were carried out while fixing the density of conical features at $1.6 \times 10^6\,cm^{-2}$ and changing the diameters of the circular pattern to 2, 3, and 4 μm. All the devices have the same size ($490 \times 292\,\mu m^2$) and epitaxial structure and were confirmed to have the same IQE performance.

*E-mail address: yujizhao@engineering.ucsb.edu

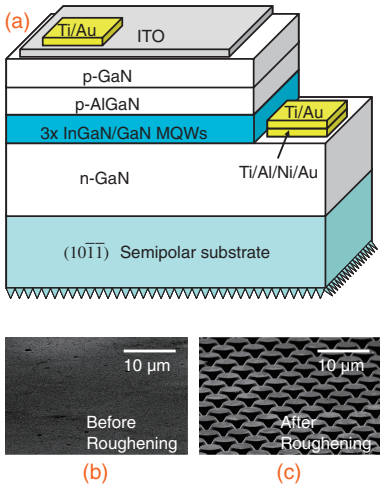

Fig. 1. (a) Schematic views of the semipolar (10$\bar{1}\bar{1}$) LED device with backside roughening structures. (b) SEM images of the backside of the GaN substrate before roughening and (c) after roughening, from a 10° tilted angle.

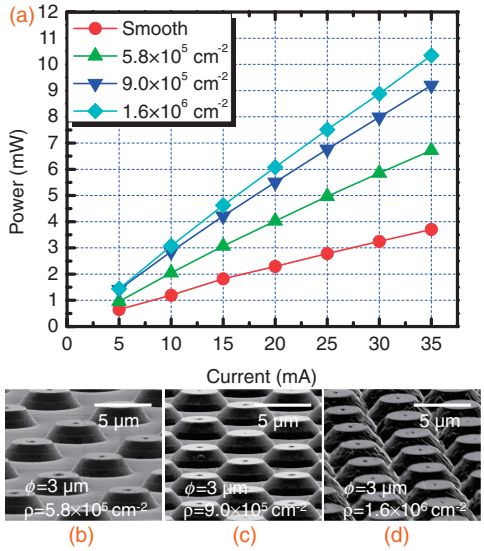

Fig. 2. (a) Dependence of light output power on the densities of the conical features patterned on the backside of the devices. (b) SEM images of the backside of the device with low density ($\rho = 5.8 \times 10^5$ cm^{-2}), (c) medium density ($\rho = 9.0 \times 10^5$ cm^{-2}), and (d) high density ($\rho = 1.6 \times 10^6$ cm^{-2}) of conical features (upper diameter $\phi = 3\,\mu$m).

Figure 2(a) shows the dependence of power on the density of the conical features. The light intensity increases significantly when the feature density is increased from 5.8×10^5 to 1.6×10^6 cm^{-2}, which showed that η_{extr} is very sensitive to the density of the features. At a driving current of 20 mA, the roughened devices had a 75, 140, and 165% increase in output power for features densities of 5.8×10^5, 9.0×10^5, and 1.6×10^6 cm^{-2}, respectively, compared with the reference device with a smooth surface. Figures 2(b)–2(d) present SEM images of the roughened backsides with low density ($\rho = 5.8 \times 10^5$ cm^{-2}), medium density ($\rho = 9.0 \times 10^5$ cm^{-2}), and high density ($\rho = 1.6 \times 10^6$ cm^{-2}), in which the amount of flat space between the conical features decreases greatly with higher feature density.

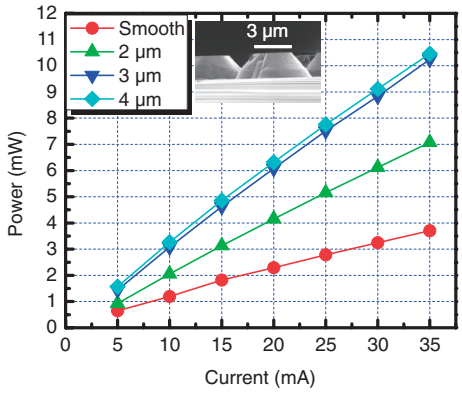

Fig. 3. Dependence of light output power on the size of the conical features patterned on the backside of the devices. Inset: Cross-sectional SEM image of the backside of the device, indicating a conical feature with an upper diameter of 3 μm.

Figure 3 demonstrates the dependence of output power on the size of the conical features at a density of 1.6×10^6 cm^{-2}. The inset of Fig. 3 is a cross-sectional SEM image of the roughened backside with 3 μm upper diameter size. As one can see, the power increases when the upper diameter of the feature increases from 2 to 3 μm, but saturates at 4 μm. It appears [from Fig. 2(d)] that increasing the density of features beyond 1.6×10^6 cm^{-2} at a diameter of 3 μm will only result in an overlap of the cone features at their base, and is unlikely to significantly improve the power.

Light extraction based on Monte Carlo ray tracing was carried out to simulate the above described experiments, using LightTools 7.0 from Optical Research Associates. The simulation model had the device structure depicted in Fig. 1(a), where the absorption coefficients (α) of each layer are as follows: $\alpha_{GaN} = 2\,\text{cm}^{-1}$, $\alpha_{n\text{-}GaN} = 75\,\text{cm}^{-1}$, $\alpha_{p\text{-}GaN} = 100\,\text{cm}^{-1}$, $\alpha_{ITO} = 500\,\text{cm}^{-1}$. The active region has an absorption value dependent on wavelength, where the value at the peak wavelength is 20 cm^{-1}. Metal contacts/pads were considered to be completely absorbent. 50,000 light rays were generated in the device active region to achieve convergence in the resulting data. Photons were emitted to conform to a standard Gaussian distribution with a central wavelength of 455 nm and a full-width at half-maximum (FWHM) of 15 nm. All the surfaces utilized full Fresnel equations and incorporate a probabilistic ray splitting approach.

Figures 4(a) and 4(b) show the simulated and actual results of the two experiments. Both sets of data were plotted as the η_{extr} enhancement, which is defined as the power of the roughened surface over the power of the smooth surface, versus feature density or size. The experimental results share the same trend as the simulation data, where, in both cases, the enhancement of η_{extr} first increases with increased density or size and then saturates at an optimal value, most likely due to the elimination of the flat surface between the conical features. The simulation data of η_{extr} enhancement peaks at a 4 μm diameter, which is consistent with the experiment result, while the density series suggest a more condensed feature density (2.0×10^6 cm^{-2}) compared with the experiment data (1.6×10^6 cm^{-2}), which could be beneficial to further improve the device performance. The simulation is based on the *c*-plane and does not include any polarization or

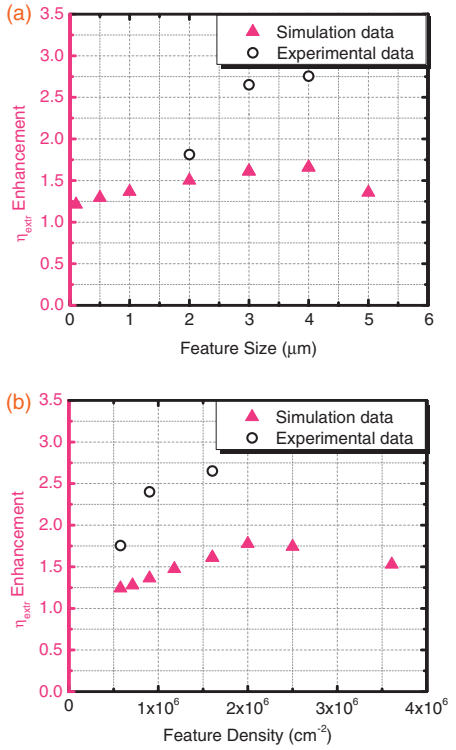

Fig. 4. Simulation and experimental data on η_{extr} enhancement vs (a) density and (b) size of the conical features.

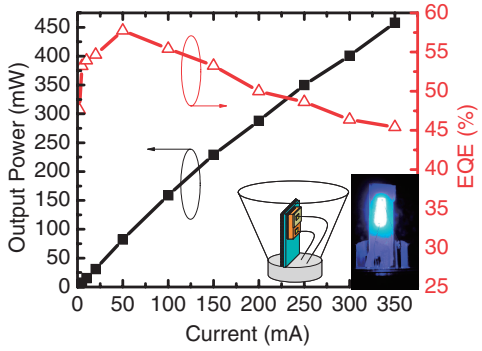

Fig. 5. Light output power vs current (*L*–*I*) and external quantum efficiency vs current (EQE–*I*) curves for a packaged ($10\bar{1}\bar{1}$) LED with backside roughening under pulsed conditions. Insets: Schematic graph (left) and optical micrograph (right) of a working blue LED using a transparent packaging method.

birefringence, which explains the difference between the measured value of η_{extr} enhancement and simulation results. A more thorough simulation study, including the polarization of spontaneous emission, is a subject of ongoing investigation.

Finally, we fabricated a blue LED on a semipolar ($10\bar{1}\bar{1}$) GaN substrate. The LED has the same structure as that shown in Fig. 1(a), except that it has a mesa size of $500 \times 2000\,\mu m^2$. The backside of this LED was patterned with a mask with 4-μm-diameter conical pattern with a feature density of $1.6 \times 10^6\,cm^{-2}$ and etched for 30 min. It was then diced and packaged using a vertical stand transparent packaging method.[27] A schematic graph (left) and an optical micrograph (right) of a working blue LED using this packaging method are shown as insets in Fig. 5. Room temperature (RT) electroluminescence (EL) measurements under pulsed conditions with a duty cycle of 1% were performed in an integrating sphere. Figure 5 shows the light output power vs current (*L*–*I*) and external quantum efficiency vs current (EQE–*I*) curves of the LED. At a forward current of 20 mA, the semipolar LED has an output power of 31.1 mW and an EQE of 54.7%. At 350 mA, the LED has a slightly lower EQE of 45.4% and an output power of 458 mW. All of the above numbers are the highest ever reported for semipolar or nonpolar LEDs, and are comparable to those of the best state-of-the art *c*-plane LEDs. Moreover, the roughened devices demonstrated a better performance by having a sixfold increase of the output power after packaging, compared with a fourfold increase in the case of conventional devices mainly due to the dramatic enhancement of photon extraction from the backside of the substrate.

In conclusion, a 30-mW-class high-power (i.e., around 55% EQE) blue semipolar ($10\bar{1}\bar{1}$) LED was first demonstrated using a backside roughening technique by chorine-based dry etching and an optimized epitaxial device structure. A systematic study on the effect of density and size of the conical feature on light extraction was carried out, indicating that a 4 μm diameter and higher density ($\sim 2 \times 10^6\,cm^{-2}$) of the features are beneficial for enhancing light extraction. Our work shows that semipolar devices are now capable of competing with *c*-plane devices in the visible spectrum, and with future optimization, higher performance can be expected from these devices.

Acknowledgments The authors acknowledge the support of Solid State Lighting and Energy Center at UCSB. A portion of this work was done in the UCSB nanofabrication facility, part of the National Science Foundation (NSF) funded National Nanotechnology Infrastructure Network (NNIN). This work made use of Materials Research Laboratory (MRL) Central Facilities supported by the Materials Research Science and Engineering Center (MRSEC) Program of the National Science Foundation under award No. DMR05-20415.

1) S. Nakamura *et al.*: Appl. Phys. Lett. **64** (1994) 1687.
2) F. Bernardini and V. Fiorentini: Phys. Status Solidi B **216** (1999) 391.
3) A. Hangleiter *et al.*: MRS Internet J. Nitride Semicond. Res. **3** (1998) 15.
4) A. E. Romanov *et al.*: J. Appl. Phys. **100** (2006) 023522.
5) S. Chichibu *et al.*: Appl. Phys. Lett. **69** (1996) 4188.
6) P. Walterweit *et al.*: Nature (London) **406** (2000) 865.
7) A. Chitnis *et al.*: Appl. Phys. Lett. **84** (2004) 3663.
8) A. Chakraborty *et al.*: Appl. Phys. Lett. **85** (2004) 5143.
9) A. Chakraborty *et al.*: Jpn. J. Appl. Phys. **45** (2006) 739.
10) M. Schmidt *et al.*: Jpn. J. Appl. Phys. **46** (2007) L126.
11) R. Sharma *et al.*: Appl. Phys. Lett. **87** (2005) 231110.
12) H. Masui *et al.*: Jpn. J. Appl. Phys. **45** (2006) L904.
13) K. Okamoto *et al.*: Jpn. J. Appl. Phys. **45** (2006) L1197.
14) S. H. Park and D. Ahn: Appl. Phys. Lett. **90** (2007) 013505.
15) H. Sato *et al.*: Appl. Phys. Lett. **92** (2008) 221110.
16) H. Zhong *et al.*: Appl. Phys. Lett. **90** (2007) 233504.
17) M. Funato *et al.*: Jpn. J. Appl. Phys. **45** (2006) L659.
18) Y. Zhao *et al.*: Jpn. J. Appl. Phys. **49** (2010) 070206.
19) I. L. Koslow *et al.*: Jpn. J. Appl. Phys. **49** (2010) 080203.
20) T. Nishida *et al.*: Appl. Phys. Lett. **79** (2001) 711.
21) T. Fuji *et al.*: Appl. Phys. Lett. **84** (2004) 855.
22) M. Yamada *et al.*: Jpn. J. Appl. Phys. **41** (2002) L1431.
23) D. Morita *et al.*: Phys. Status Solidi A **200** (2003) 114.
24) C. Huh *et al.*: J. Appl. Phys. **93** (2003) 9383.
25) H. Kasugai *et al.*: Jpn. J. Appl. Phys. **44** (2005) 7414.
26) H. Zhong *et al.*: Jpn. J. Appl. Phys. **48** (2009) 030201.
27) C. C. Pan *et al.*: Jpn. J. Appl. Phys. **49** (2010) 080210.